

Antibacterial Properties of Nanoparticles: A Comparative Review of Chemically Synthesized and Laser-Generated Particles

J. J. Naddeo^{1,†}, Matthew Ratti^{1,†}, Sean M. O'Malley^{1,3}, Julianne C. Griepenburg¹,
Daniel M. Bubb^{1,3}, and Eric A. Klein^{2,3,*}

¹Department of Physics, ²Department of Biology, and ³Center for Computational and Integrative Biology,
Rutgers University-Camden, Camden, NJ 08102, USA

Nanomaterials have recently received an enormous amount of attention from the scientific community due to their outstanding activity relative to bulk materials. This increase in activity relative to bulk materials can be attributed to the high surface area to volume ratio associated with nanoparticles. Nanoparticles have found applications in almost every field of science. Currently there is significant interest in the development of nanoparticles as antibacterial agents. This work is paramount due to the increasing number of antibiotic-resistant strains of bacteria. Nanoparticles can be synthesized using various methods, each with their own advantages and disadvantages, and the method is often chosen based on the intended application. This review will cover the most prevalent method, chemical-based reduction of salts, and a fairly new laser-based method that holds tremendous promise in nanoparticle synthesis. We conclude with a comparison of the antimicrobial activities of materials made via each method.

Keywords: Nanoparticles, Pulsed Laser Ablation in Liquids, Chemical Synthesis, Antibacterial.

CONTENTS

1. Introduction to Pulsed Laser Ablation in Liquids (PLAL)	1044
1.1. Laser Parameters	1046
1.2. Laser Interaction with NPs in Solution	1049
2. Wet-Chemical Method of Producing Metallic Nanoparticles	1049
2.1. Nucleation	1049
2.2. Seed	1050
2.3. Formation of Nanoparticles	1050
2.4. Controlling Nanoparticle Size	1050
3. Antimicrobial Properties of NPs	1051
3.1. Salts versus NPs	1051
3.2. Influence of NP Size	1051
3.3. Mechanisms	1052
3.4. Comparison of Wet-Chemistry and PLAL	1054
4. Conclusion and Outlook	1055
Acknowledgments	1055
References and Notes	1055

1. INTRODUCTION TO PULSED LASER ABLATION IN LIQUIDS (PLAL)

Nanoparticles (NPs) are generally classified as particles that have at least one dimension that is less than 100 nm

in length; the current increase in interest in NPs from the scientific community is due to their extraordinary range of physical properties.¹ One of the more recently developed methods for nanoparticle synthesis uses laser ablation of solid metal targets immersed in a liquid medium (pulsed laser ablation in liquids—PLAL, shown in Fig. 1). In PLAL, a bulk target is placed in a liquid environment and ablated by an incident laser pulse. A criterion for the liquid itself is that it should not have a strong absorption coefficient at the incident laser wavelength. Upon ablation of the target, a dense plume of atomic clusters and vapor is ejected into the liquid medium wherein NPs rapidly form. This methodology produces small, relatively monodisperse, surfactant-free NPs and has many advantages, namely, that it can be carried out without the need for toxic chemical precursors. Even though there have been recent efforts to develop “greener” chemical NP synthesis methods,^{2–4} chemical-based approaches still typically require the use of toxic reducing agents, such as borohydrides and hydrazines as well as capping agents like polyvinylpyrrolidone (PVP). These methods

*Author to whom correspondence should be addressed.

†These two authors contributed equally to this work.



J. J. Naddeo received his B.S. degree in physics from Rutgers University-Camden. His main research interests are laser ablation in liquids and the development of novel antimicrobial therapeutics.



Matthew Ratti is an undergraduate physics major at Rutgers University-Camden. His main research interests are laser ablation in liquids and the development of novel antimicrobial therapeutics.



Sean M. O'Malley received his Ph.D. in applied physics from the New Jersey Institute of Technology and Rutgers University. He is currently an Assistant Professor of Physics at Rutgers University-Camden and his research interests include synchrotron-based X-ray diffraction of novel device structures, composite nanoparticle systems with unique functionality, and laser-material interactions with an emphasis in ablation.



Julianne C. Gripenburg received her Ph.D. in chemistry from the University of Pennsylvania. She is currently a postdoctoral scientist and instructor in the physics department at Rutgers University-Camden. Her primary research interests are nanoparticle synthesis and derivitization.



Daniel M. Bubb received his Ph.D. in physics from the New Jersey Institute of Technology and was a postdoctoral fellow at the Naval Research Laboratory. He is currently a professor and chair of the Physics Department at Rutgers University-Camden. His research interests include laser processing, laser-materials interactions, thin film deposition and characterization, non-linear optical properties of nanoparticles and nanocomposites, ferroelectricity, superconductivity, and properties of novel oxides.



Eric A. Klein received his Ph.D. in pharmacology from the University of Pennsylvania and was a postdoctoral fellow in molecular biology at Princeton University. He is an Assistant Professor of Biology at Rutgers University-Camden. His research interests include bacterial cell shape, host-pathogen interactions, and the development of novel antimicrobial therapeutics.

violate a number of Green Chemistry Principles including: developing less hazardous chemical syntheses, utilizing safer solvents, and reduction of derivatives.^{5,6} Conversely, PLAL provides an environmentally responsible option for nanoparticle synthesis that satisfies all 12 of the Principles of Green Chemistry.^{6,7} NPs produced by PLAL are finely dispersed in an aqueous medium and the size, polydispersity, and composition of the synthesized NPs can be easily controlled by the composition of the aqueous ablation liquid.^{7–11} While the primary focus of this review is on ablation in a liquid medium, another noteworthy technique is gaseous medium laser ablation (GMLA).^{12–14}

While this review provides a comprehensive introduction to the PLAL field, there are several topics that are not covered that readers should be aware of. The first is the addition of chemicals to the liquid medium, which can serve to control the size, polydispersity, and

composition of the synthesized NPs.^{7–11} Second, is the formation of a cavitation bubble that contains a large portion of the ablated material and/is where initial particle growth ensues. For further discussion on the role of the cavitation bubble in PLAL the reader is directed to these fine reviews and research articles.^{7,9,10,15–23}

1.1. Laser Parameters

As previously mentioned, laser ablation provides the ability to tune nanoparticle characteristics; this can be done through adjusting a number of laser parameters, including: fluence, wavelength, and pulse duration. Here we describe the relationship between laser parameters and synthesized NP properties.

1.1.1. Fluence

Laser fluence is defined as the pulse energy divided by the area of the laser spot on the target surface. When considering the laser fluence, one must take care to properly specify the beam size, using a protocol that can provide an accurate measurement, e.g., the knife-edge method. In quantifying the effect of the fluence, one can make reference to different “regimes.” Each of these regimes is defined loosely as a fluence range that is dominated by a specific ablation mechanism. Within a given regime, the production rate of NPs increases linearly with fluence.^{24,25} However, the exact effects of fluence on the size and polydispersity of the produced NPs are the subject of considerable discussion in the literature. Some of this division comes from the very loose definition of what constitutes the labels “high” and “low” as applied to fluence. Moreover, confusion can be compounded by the use of ‘ultra-short’ (often referred to in literature as ‘ultra-fast’) lasers, where multiple non-linearities are often present. Our discussion will begin with ‘long’ pulse length, nanosecond (*ns*), lasers. These are the most prevalent type of pulsed laser systems because of their relative cost and ease of use.

In a study in which *ns* lasers were utilized, a negative linear relationship between size and fluence was observed for gold in distilled deionized (DDI) H₂O, irradiated with a low fluence, ranging from 4–35 J/cm².²⁶ This trend is attributed to ablation dominated by thermal vaporization, where NPs are produced via a bottom-up nucleation

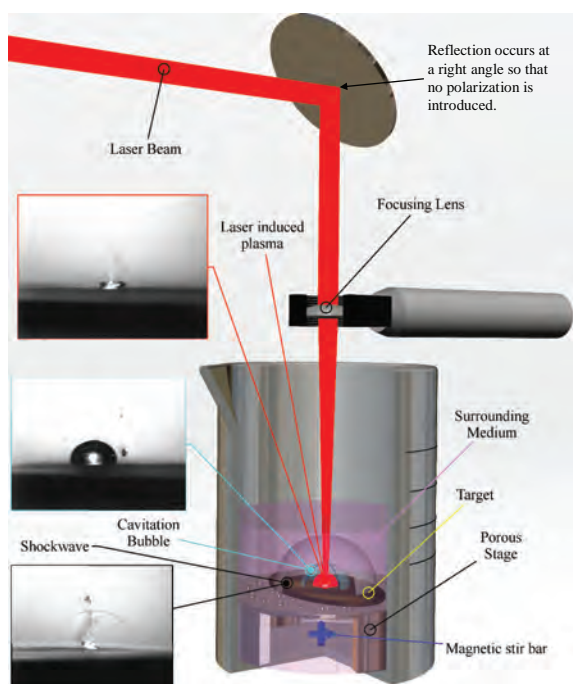


Figure 1. Typical PLAL set-up. Inserts are shadowgraph images of plasma, cavitation bubble, and shockwave of gold submerged in distilled deionized (DDI) H₂O irradiated with a Nd:YAG laser with a pulse duration of 25 ps operating at the fundamental wavelength ($\lambda = 1064$ nm).

process.²⁷ For the same target-solvent system, a critical fluence of 35 J/cm² can be defined, wherein the relationship between size and fluence remains linear but the slope becomes positive. Elsayed et al. showed that particles made at 35, 53, 70, and 88 J/cm² produced particles with diameters of 8, 11, 13, and 14 nm, respectively.²⁶ It was also shown experimentally for nanosecond ablation, where the fluence ranged from 46 J/cm² to 140 J/cm², that lower fluences produce smaller more monodisperse particles whereas higher fluences produce larger NPs that are polydisperse.²⁸ The reason for these experimental findings is still vigorously debated in literature. One explanation is that the use of higher fluences extends the lifetime of the cavitation bubble, and thus allows a longer time for NPs to coalesce, and become larger. It was also proposed that the use of a higher fluence induces an explosive boiling, a top-down mechanism, that ejects molten NPs directly into the medium.²⁷ When employing fluences higher than the aforementioned critical point, one can expect to see a higher concentration of ejected material, which can feed further particle growth. Often, the increase in particle size with fluences above the critical point is accompanied by a bimodal size distribution.²⁸ This may result from absorption of the incident beam by NPs in the optical path as it propagates through the liquid layer. Secondary absorption can lead to particle fragmentation, increasing the population of smaller particles.

The second system we will examine is ‘ultra-short’ lasers (10 fs–1 ps). Experiments show that for a 110 fs pulsed laser there exists a positive linear relationship between fluence, size, and polydispersity, in the range of 60 J/cm² to 1000 J/cm². However, for fluences a few J/cm² above the ablation threshold the relationship switches from positive to negative. Povarnitsyn et al. have performed numerical simulations of the PLAL process using a hydrodynamic two-temperature model.^{17,29} Their model of a 200 fs laser ablating an Au target in water reveals that for fluences at, or slightly above, the ablation threshold the dominating ejection mechanism is spallation. Spallation results in the ejection of a metastable molten layer, which breaks apart due to Rayleigh instabilities, at low fluence, leading to the formation of NPs with sizes comparable to the thickness of the spalled layer. As the fluence increases, the ejected material undergoes phase explosion, thus producing smaller particles.^{17,29} Polydisperse samples are produced at very low fluences, due to erratic ablation caused by irregular absorption from impurities and nanostructuring in the target material.³⁰ This is especially true for wavelengths of incident light that are weakly absorbed by the target material.

In summary, PLAL produces bimodal size distributions due to the presence of multiple ablation mechanisms. If only one mechanism is present, the relationship between fluence and polydispersity is usually found to be linear. In general it has been shown that for ‘long’ and ‘ultra-short’ pulsed laser systems there are low and high fluence

regimes that produce negative and positive trends in size, respectively.^{17,26,27,31}

1.1.2. Wavelength of Incident Laser Light

Given the complex interactions between high-intensity lasers and liquids, ablation media are chosen that do not strongly absorb or scatter the operational wavelength. Non-linear interactions in crystals can allow the laser output to be tuned over a fairly broad range. The interactions between the ablation liquid and laser output will be discussed later in this section. Here, we focus on nanosecond pulsed lasers due to the complexity of *fs* and *ps* ablation.

There are numerous mechanisms that must be taken into account when selecting a wavelength. For instance, it has been shown experimentally that wavelengths that are strongly absorbed by the target material will suffer from shielding effects caused by plasma and particles in the optical path.^{28,32,33} Evidence of shielding can be seen by an increase in ablation efficiency or mass yield of NPs when near-IR lasers are used instead of visible or UV lasers.^{27,34} Recent experiments show that at shorter (UV) wavelengths the incident photons have enough energy ($E > 3.49$ eV) to cause photo-ablation via the breaking of molecular bonds, thus circumventing common thermal ablation pathways.³⁵ Table I presents the photon energies of commonly used laser wavelengths (A) and the bond energies of common metallic targets (B). Photo-ablation is considered an example of a top-down mechanism for the formation of NPs because the breaking of bonds causes ultra-small fragments of material to be ejected into, and quenched by, the surrounding liquid, producing larger more polydisperse samples.^{35–37} Conversely, near IR ablation ($\lambda = 1064$ nm) is considered to be a more bottom-up approach due to the fact that it is dominated by plasma ablation.³⁵ The target can interact with the incident pulse via Inverse Bremsstrahlung (IB) absorption, causing cascade ionization, also known as electron avalanche. This absorption frees electrons that collide

Table I. Bond energies of common target metals (A)¹³⁵ compared to photon energies of wavelengths used for ablation (B).

A Metal	B				
	Bond energy (eV)	Laser system	Laser pulse duration	Wavelength (nm)	Photon energy (eV)
Ag	2.92	ArF	10 ns	193	6.42
Au	3.46	Nd:YAG	5–25 ns	355	3.49
Cu	3.48			532	2.33
Pd	3.89			1064	1.17
Pt	5.83	Ti:Sapphire	3 ps–10 fs	800	1.55

Notes: Nonlinear effects, such as two photon absorption, can cause photo ablation to occur even when the incident photons have a lower energy than the bond energy of the target material. The probability of nonlinear effects being present increases as the intensity of the incident light increases. The intensity of a laser is the fluence divided by the pulse duration, therefore lasers capable of producing ultrashort pulses (fs/ps) tend to photo ablate even when the operational wavelength is high. Nanosecond lasers can also ablate via nonlinear mechanisms at high fluences.

with, and subsequently free, bound electrons. As collisions increase, so do the number of free electrons, which further the collision process, thus freeing more bound carriers. This “avalanche” process ionizes the material, thus igniting a plasma. As shown by Eqs. (1) and (2) below, the IB absorption coefficient, σ_{IB} , is proportional to the cube or square of the wavelength of incident photons, for ion-electron and atom-electron IB absorption respectively.^{38–40}

Ion-Electron:

$$\sigma_{IB}(\lambda) = \frac{3.7 \times 10^{18}}{T_e^{1/2} \nu^3} Z^2 \left[\exp\left(\frac{h\nu}{k_B T_e}\right) - 1 \right] n_e n_i \quad (1)$$

$$\text{Atom-Electron: } \sigma_{IB}(\lambda) = \frac{e^2}{\pi m_e c \nu^2} n_e n_0 \sigma_{\text{col}} \left(\frac{8k_B T_e}{\pi m_e} \right) \quad (2)$$

$$\lambda = \frac{c}{\nu} \quad (3)$$

In the above equations, ν is the laser irradiation frequency, which is related to the wavelength by Eq. (3), T_e is the electronic temperature, n_e , n_i , and n_0 are the number densities of the electrons, ions, and neutral atoms, respectively, m_e is the electron mass, Z is the ionic charge, h is Planck’s constant, k_B is the Boltzmann constant, c is the speed of light in a vacuum, and σ_{col} is the cross-section for electron–neutral atom collisions.³⁹ The surrounding liquid confines the plasma (Fig. 1) and increases its lifetime allowing for more interaction with the tail end of the laser pulse, thus further increasing IB absorption.³⁵ This process causes the temperature and pressure of the plasma to increase. The expanding plasma is quenched by the surrounding liquid and condenses into NPs with various geometries.^{9, 35, 41} Some of these NPs will still have enough energy to sinter together and form larger particles.^{27, 42} As the initial temperature of the plasma increases the probability of agglomeration will also increase. This is one explanation for why longer wavelengths produce larger NPs.^{7, 37} As previously discussed, absorption of the incident pulse by the NPs in solution is a mechanism that can lead to a reduction in size, especially when the NP’s extinction coefficient is high at the wavelength of the incident photons.^{32, 43, 44} This secondary irradiation effect will be covered in more detail below.

1.1.3. Pulse Width of Incident Laser Pulse

The temporal width of the laser pulse plays a critical role in PLAL. In this section, we will split pulsed lasers into two broad categories based on their pulse width. The first class of lasers has pulse durations greater than a few *ps*, and is usually called ‘long-pulsed.’ In this case, the laser pulse duration is longer than the electron-phonon equilibration time, which is typically on the order of a few picoseconds.^{9, 45–49} When the laser pulse is longer than this relaxation time, some of the energy from the laser pulse will diffuse into the surrounding lattice before the onset

of ablation, allowing energy to be dissipated into the surrounding liquid. This leaking of energy induces heating in the surrounding material, which results in formation of a heat affected zone (HAZ).^{9, 50, 51} Lasers that exhibit this behavior include all milli (*ms*), micro (μs), nano (*ns*) and some picosecond (*ps*) pulsed lasers. The ablation process in these cases is dominated by thermal mechanisms such as thermionic emission, vaporization, boiling and melting.^{7, 51} As discussed in the previous section, longer pulses allow for the laser pulse to interact with the produced plasma, increasing its temperature, pressure and thus lifetime.^{7, 51}

The second class of lasers will be referred to as ‘ultra-short’ and consists of lasers with pulse durations less than a few picoseconds. These short pulse durations ensure that excited electrons do not interact with the surrounding lattice,^{45, 47–49, 52–54} thus allowing for much more precise delivery of energy to the target material and minimizing the spread of a HAZ. Thermal confinement is regularly exploited in nano-scale laser machining.^{9, 50–52, 55–57} Ultra-short lasers can produce intensities that induce nonlinear effects to occur such as multiphoton ionization and tunneling photoionization.⁵² These nonlinear effects can cause avalanche photoionization as well. The Keldysh parameter (γ) can be represented for both atoms and bulk dielectric materials. Keldysh first laid the theoretical framework for determining whether multiphoton or quantum tunneling will dominate when dealing with atoms exposed to intense electromagnetic fields in 1965 with the following Eq. (4),⁵⁸

$$\gamma = \frac{\omega}{e} \sqrt{\frac{m_e c \epsilon_0 E_{\text{ion}}}{I}} \quad (4)$$

where, ω is the laser angular frequency, I is the laser intensity at the focal point, E_{ion} is the ionization energy of the atom, m_e is the effective electron mass, e is the fundamental charge of an electron, c is the speed of light in a vacuum, and ϵ_0 is the dielectric constant in a vacuum. The Keldysh parameter γ defines the transition between the two limiting regimes of nonlinear ionization (multiphoton or tunneling); $\gamma = 1$ denotes the demarcation line. Assuming $\hbar\omega < E_{\text{ion}}$, if $\gamma > 1$ (ionization with high frequency and rather low intensity) multiphoton absorption is expected to be operating; tunneling ionization occurs if $\gamma \ll 1$ (low laser frequency, high intensity). Importantly, the Keldysh parameter equation can be modified to handle a variety of experimental conditions including bulk dielectric media.^{52, 59, 60}

We note that modern ultrafast lasers enable a third process called over-the-barrier ionization (OTBI) in which sufficiently intense laser fields, irrespective of laser frequency, lower the potential barrier to such an extent that the electron can cross over the barrier without tunneling.⁶¹ Ultra-short lasers usually produce polydisperse samples with larger size, while nanoparticles produced by ‘long’ pulsed lasers are smaller and more monodisperse.^{7, 62, 63} The monodisperse nature of NPs synthesized by long-pulsed lasers is a result of the temporal overlap of the

plasma and the laser pulse. As stated earlier, this overlap will induce a more bottom-up formation process, via a hotter plasma, thus aiding in the production of smaller more uniform NPs. Conversely, the polydispersity of NPs produced with ‘ultra-short’ pulsed lasers is a result of the photo-ablation caused by the nonlinear mechanisms mentioned earlier. This is confirmed by computational studies which demonstrate that ‘ultra-short’ lasers cause fragments of metal to be ejected, leading to large variations in size.⁶⁴

1.2. Laser Interaction with NPs in Solution

As discussed above, laser parameters must be carefully chosen so that the liquid medium does not absorb an appreciable fraction of the pulse’s energy. A major assumption made is that the ablation medium is considered “pure,” having a negligible amount of absorbing impurities. However, the process of PLAL produces colloidal nanoparticles, which, depending on their composition and morphology, can absorb UV to IR light, thus increasing the solutions opacity. The media in Figure 1 depicts colloidal Au NPs, which absorb strongly in the visible range (as evidenced by their pinkish hue). It has been extensively shown in the literature that NPs produced from prior ablation can effectively shield the target from the incident laser, thus reducing the amount of energy delivered to the target.^{28,32,33} Barcikowski et al. showed that flowing a liquid over the target increased the production rate by a factor of four and greatly enhanced experimental reproducibility, by reducing this shielding effect.⁶⁵ Our group uses magnetic stir bars (Figs. 1–2) and has observed similar results, with respect to reproducibility. Secondary irradiation is frequently used to change the properties of the produced NPs. Our lab has extensively used secondary irradiation (post-irradiation) of colloidal NP solutions to decrease the size and increase the uniformity of

the colloidal solution.²² Mafune has also shown that novel nano-solders can be engineered using a post-irradiation step typically referred to as pulsed laser irradiation (PLI).⁶⁶

A typical experimental apparatus for PLI is represented in Figure 2. A laser wavelength is selected to be close to an absorption peak of the colloidal solution. Ultra-fast laser systems can produce a super continuum, as long as the peak power is above 4.4 MW, which allows for lasers with wavelengths not absorbed by the NPs to be used in PLI.^{42,67} Current models suggest that NPs absorb incident photons fragment via two competing mechanisms

- (i) Photo thermal evaporation and melting or
- (ii) Coulombic explosion.^{22,42,53}

Coulombic explosion occurs when the NPs encounter a high-intensity field (usually from an ‘ultra-short’ pulse) and electrons are quickly ejected from the NP. The left-over positively charged regions experience strong repulsive forces that induce fragmentation. Coulombic explosion has been attributed with being the dominant mechanism when ‘ultra-short’ pulsed lasers are used.^{22,42,68,69} When metal NPs are irradiated with *ns* lasers with a wavelength near the particle’s surface plasmon resonance, the absorbed photons excite electrons that then relax rapidly and excite phonon modes.^{70,71} Photo-thermal heating can induce temperatures above the NP’s melting point but below the vaporization point, leading to molten particles that can merge to form larger particles. At even higher temperatures, size reduction can occur due to vaporization.⁷⁰ In order to enhance this size reduction, it has been shown that adding agents such as polyvinylpyrrolidone (PVP) to the solution can greatly enhance post-irradiation effect.¹⁰ Additives that enhance the PLAL process will not be discussed in this article, as the field is much too large and would be beyond the scope of this review. However, the reader is directed to additional reviews that discuss the effects of various solutes as well as changing the solvent matrix.^{7–9}

2. WET-CHEMICAL METHOD OF PRODUCING METALLIC NANOPARTICLES

2.1. Nucleation

Wet-chemistry is the traditional method used to produce NPs and is considered a bottom-up synthesis process. This method provides the ability to control morphology, crystallinity, and composition. The chemical reduction of salts allows for significantly larger NP yields relative to the aforementioned PLAL method.⁷² For example, Barcikowski et al. showed that using a flow cell in conjunction with a high repetition rate picosecond pulsed laser, silver NP production rates of 31.0 mg/hr are achievable.⁶⁵ Our group was able to obtain Ag NP production rates, using a 250 Hz ps-laser and a more conventional PLAL setup as shown in Figure 1, of around 10 mg/hr. In contrast, Swain et al. showed that with an optimized

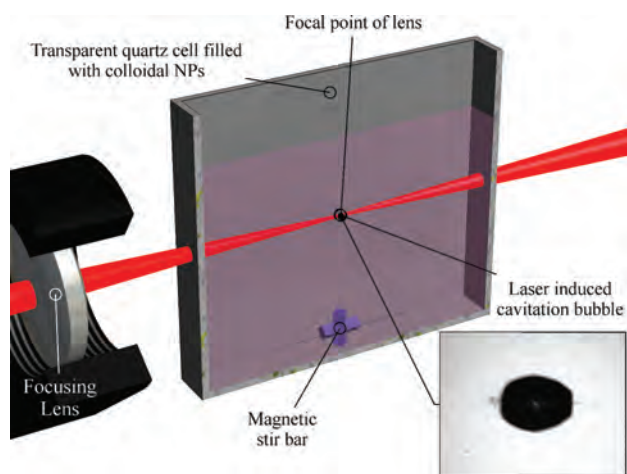


Figure 2. Typical post-irradiation set-up. Insert is shadowgraph of cavitation bubble induced in distilled deionized (DDI) H₂O by Nd:YAG laser with a pulse duration of 25 ps operating at the second harmonic wavelength ($\lambda = 532$ nm).

chemical synthesis set up production rates of cobalt NPs can reach 1 kg/hr.⁷³ The basis of wet chemical synthesis begins with the nucleation process, in which a particle of a new phase forms in a previously single-phase system, such as a homogenous salt solution.⁷⁴ This particle is labeled a “seed.”⁷⁵ From this seed, further growth to obtain a NP is possible with the addition of metal atoms. Varying reaction conditions, such as reducing agent and salt concentrations, temperature, and reaction time all affect the growth and shape of the NP formed.^{73, 76–78}

2.2. Seed

The formation of a seed begins with the reduction of a salt (see Table II for a list of common reducing agents and salts).⁷⁹ The concentration of atoms increases as the precursor decomposes until the total concentration reaches a supersaturated state.⁸⁰ At this supersaturated state the atoms begin to aggregate and form nuclei that evolve into a seed (Fig. 3).⁸⁰ Typically, salts such as sodium citrate and sodium dodecyl sulfate, and polymers such as polyvinylpyrrolidone (PVP), are used as capping agents.^{72, 79, 81} Capping agents help to stabilize the metallic seed by maintaining size and preventing agglomeration.^{82, 83} Once the seed is formed, additional metal atoms can be added to produce the nanocrystal. Seed-mediated growth is a preferred method due to the low activation energy required for metal reduction on to the preformed seeds.⁸⁴ Additionally, seed-mediated growth is one of the most effective and efficient ways of controlling the size and shape of NPs.^{84, 85}

2.3. Formation of Nanoparticles

The formation of a nanocrystal, or nanoparticle, is controlled by the competition between an increase in surface energy and a decrease in bulk energy.⁸⁰ An increase in the surface energy favors dissolution while a decrease in bulk energy favors growth.⁸⁰ Continued atomic-addition allows for the seed to increase in size in a relatively uniform

fashion. The existing seeds will continue to grow into a NP by diffusion-driven deposition onto the surface of the seed.⁸⁶ A spherical particle is formed using a simple salt, metal precursor and capping agent solution. Morphological variations can be introduced at this seed stage, but the primary focus in this review is on spherical/globular NPs.

2.4. Controlling Nanoparticle Size

There are a variety of methods used to control the size of NPs produced by wet-chemical synthesis. A common method of producing small monodisperse NPs is by citrate reduction of a metallic salt.^{83, 87, 88} Ag NPs produced using sodium citrate as a reducing agent range from 50–100 nm in diameter, while NPs with a size of 5–20 nm can be obtained by using the stronger reducing agent sodium borohydride.⁸⁷ In addition to reducing agent selection, concentration of the reducing agent also plays a critical role. Increased concentration of sodium citrate increases the amount of Ag⁺ reduction, and allows for slow growth of Ag NPs and larger particle size.⁸⁷ In the case of Cu NPs, increasing the ratio of reducing agent to salt precursor while increasing the pH decreases the size of NPs produced.⁸⁹ However, when the concentration of the reducing agent is much higher than that of the metal precursor, the change in precursor has no direct effect on the size of the NP produced.⁹⁰ Size control can also be attained by controlling the pH of the reaction, often using ascorbic acid as a reducing agent, and it has been shown that increasing the pH of the reaction decreases the size of the particles.⁹¹ Capping agents also help maintain a range of sizes and shapes, and in some cases prevent oxidation.⁸⁰ A protective agent can encapsulate a particle and prevent further growth.⁸⁰ Interestingly, surfactants such as cetyltrimethylammonium bromide (CTAB) only attach to certain facets on the particle, thus favoring the formation of rods or nanowires.⁸⁹ Using a protective agent such as polyvinylpyrrolidone (PVP) or polyvinyl alcohol (PVA) during particle growth keeps Ag NP size under 100 nm, while remaining spherical in shape.⁹² Zinc oxide

Table II. Different reagents involved in the production of metallic nanoparticles via wet-chemical synthesis.

Wet-chemical synthesis reactants		
Metal salts	Reducing agents	Capping/stabilizing agents
—Zinc nitrate hexahydrate ($Zn(NO_3)_2 \cdot 6H_2O$) ⁷²	—Ascorbic acid ($C_6H_8O_6$) ^{85, 140}	—Polyvinylpyrrolidone (PVP) ^{72, 136}
—Chloroauric acid ($HAuCl_4$) ⁸¹	—Sodium borohydride ($NaBH_4$) ¹³⁶	—Bromide (Br^-) ⁸⁵
—Nickel nitrate Hexahydrate ($Ni(NO_3)_2 \cdot 6H_2O$) ¹³⁶	—Ammonium hydroxide (NH_4OH) ⁷²	—Thioglycerol ($C_3H_8O_2S$) ¹⁴⁴
—Cobalt(II) hydroxide ($Co(OH)_2$) ⁷³	— <i>o</i> -diaminobenzene ($C_6H_4(NH_2)_2$) (<i>o</i> -DAB) ¹⁴¹	—Cetyltrimethylammonium bromide (CTAB) ^{81, 141, 145}
—Copper iodide (CuI) ¹³⁷	—Dichlorodiphenyltrichloroethane (DDT) ¹³⁷	—Polyvinyl alcohol (PVA) ⁹²
—Copper acetate ($Cu(CH_3COO)_2$) ⁷⁷	—Hexamethylenetetramine ($C_6H_{12}N_4$) (HMT) ^{76, 142}	—Trisodium citrate ($Na_3C_6H_5O_7$) ¹³⁶
—Copper chloride ($CuCl_2 \cdot 2H_2O$) ¹³⁸	—Oleic acid ($C_{18}H_{34}O_2$) ¹³⁸	—Daxad 19 ¹⁴⁶
—Copper sulfate pentahydrate ($CuSO_4 \cdot 5H_2O$) ⁹⁰	—Tannic acid ¹⁴³	—Sodium dodecyl sulfate (SDS) ¹³¹
—Copper dodecyl sulfate ($Cu(DS)_2$) ¹³⁹	—Sodium citrate ⁸⁷	—Polyallylamine hydrochloride (PAH) ¹⁴⁷
—Silver nitrate ($AgNO_3$) ⁹¹	—Hydrazine hydrate ($NH_2NH_2 \cdot H_2O$) ¹³¹	—3-mercaptopropionic acid (MPA) ¹⁴⁷

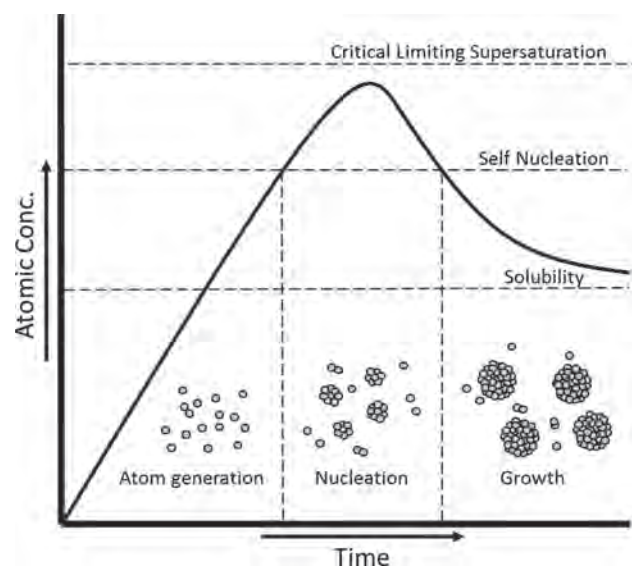


Figure 3. Generation of atoms, nucleation then growth of particle, showing atomic concentration over time.¹³⁴ Reproduced with permission from [80], Y. Xia, et al., *Angew Chemie-Int. Ed.* 48, 60 (2009). © 2009, John Wiley and Sons.

NPs of the size 6.5–8.5 nm were produced using PVP as a capping agent and smaller Ag NPs were obtained by increasing PVP concentration.^{72,93} Finally, the length of reaction also plays a role in NP size control.⁹⁴ Increasing reaction time typically increases the size of NPs, likely due to the increased addition of metal to available facets on the particle surface.^{80,85} A list of reactants and capping/stabilizing agents are shown in Table II. The importance of size control of the NPs is discussed below, as size has been shown to play a crucial role in their toxicity.

3. ANTIMICROBIAL PROPERTIES OF NPs

3.1. Salts versus NPs

The number of published articles on the toxic effects of NPs has risen dramatically since 1990; according to

Thomson Reuters ISI WoS, currently there are 3500 papers published annually on the topic.⁹⁵ For centuries metals and metallic salts have been known to have antibacterial properties. The uses of silver date back to the Chaldeans as early as 4,000 B.C.E. and Persian kings who would not drink water unless it was transported in silver containers.⁹⁶ The relatively recent advances in nano-engineering have enabled scientists to study the antibacterial properties of nanoparticles. Results from this research show that NPs are much more effective antibiotic agents than their respective bulk materials.⁹⁵ The mechanism by which these NPs induce toxicity is still the topic of much debate. The three main hypothesized mechanisms include the production of reactive oxidative species (ROS), ion release, and NP interaction with the cell membrane. In contrast to metal salts, metal NPs offer a wider range of mechanisms to combat bacterial infections; this may provide an advantage in the prevention of bacterial resistance, which is a major clinical problem for currently used antibiotics.^{97–99} It has also been shown that metal oxide NPs are more toxic than their salt precursor involving equal amounts of metal.^{100–103} In contrast to ZnO NPs, the salt precursor zinc chloride ($ZnCl_2$) showed no antibacterial activity.⁹⁷ The same result is seen with Cu NPs and $CuCl_2$.¹⁰⁴ Lastly, NPs have the capability of attaching to the cell surface.^{105,106} This attachment allows for localized effects and possible internalization.^{105,107,108}

3.2. Influence of NP Size

One of the major reasons why NPs attract so much interest is their relatively large surface area to volume ratio, which allows NPs to exhibit phenomena not observed in the bulk material. This ratio is inversely related to the radius of the particle, thus smaller particles have larger surface area to volume ratios and are considered to be more “active.” The current consensus is that in order for a particle to be considered “nano” and exhibit novel biological effects the diameter of the particle must be less than

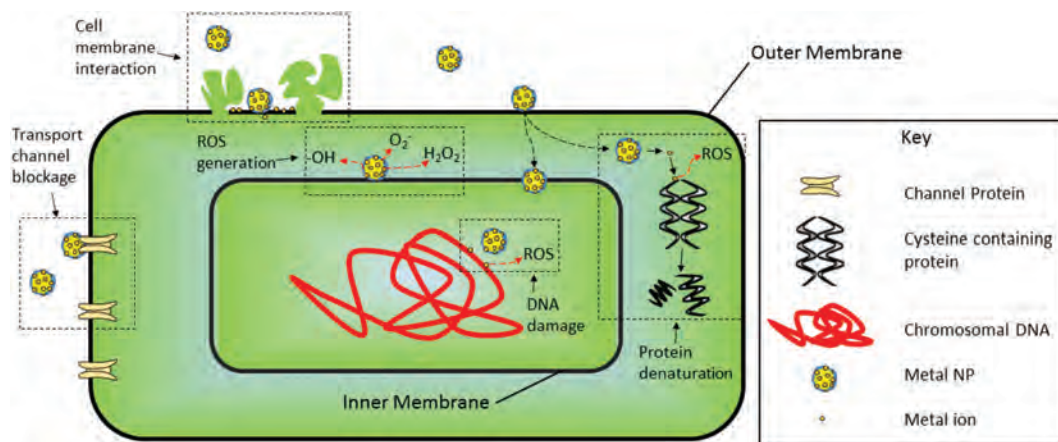


Figure 4. Graphical depiction of typical bacterial cell in presence of nanoparticles. Prominent mechanisms are highlighted.

100 nm. However, a recent study from Ivask et al. showed that the threshold for novel biological effects is closer to 20 nm for Ag NPs.¹⁰⁷ Several reports demonstrate that the antibacterial activity of NPs is strongly influenced by the NPs size.^{107, 109–111} The reasons for size-dependent toxicity have been attributed to not only the higher effective surface area, but also the ability of smaller NPs to pass through the cell's outer membrane, thus making metal ions and ROS more bioavailable within the cell.¹¹² Tables III and IV demonstrate a general trend: a decrease in nanoparticle size is often correlated with an increase in antibacterial activity. This is independent of the nanoparticle production method (wet chemistry or PLAL).

3.3. Mechanisms

3.3.1. NP Interactions with the Cell Membrane

NPs are able to attach to bacterial cells, causing structural changes in the cell membrane and possibly the blockage of transport channels.^{113, 114} As with other mechanisms

discussed earlier, this phenomenon is also size-dependent. Smaller NPs have a larger surface area to volume ratio, which allows for a higher effective interaction with the cell membrane. However, larger NPs have a higher absolute surface area allowing for better van der Waals adhesion. Thus, it can be concluded that although size plays a significant role, it is not exclusive in the determination of antibacterial efficiency; other factors such as composition are of equal importance.¹¹⁵ After attachment, NPs may be internalized, ionize within the cell, and damage intracellular structures resulting in cell death (Fig. 4).¹¹² For example, Cu NPs made with no surfactant have been observed to directly attach to the membrane, resulting in a large rate of NP oxidation.^{116–118}

3.3.2. Generation of Reactive Oxidative Species

The production of reactive oxidative species (ROS) by metal NPs plays a large role in their antibacterial effectiveness (Fig. 4). ROS consist of short-lived oxidants,

Table III. Compilation of results from antibacterial studies of NPs produced via wet-chemistry.

Metal	Bacteria	Chemical additives	Size (diameter)	Effectiveness	Source	
Ag	<i>E. coli</i>	Citrate	9 ± 2 nm ^b	9 ± 1 mm; ^d 14.38 μg/mL ^a	[108]	
		Citrate/SDS	30 ± 7 nm ^b	26 ± 0.5 mm; ^d 215.74 μg/mL ^a	[108]	
		Gallic acid	20–25 nm ^b	0.5 ± 0.2 μg/mL ^a	[148]	
			7 nm ^{a, b}	6.25 μg/mL ^a	[130]	
			29 nm ^{a, b}	13.02 μg/mL ^a	[130]	
		Lactose	35 nm ^{a, b}	27.0 μg/mL ^{a, c}	[115]	
			Maltose	25 nm ^{a, b}	3.38 μg/mL ^{a, c}	[115]
			SDS	24 ± 6 nm ^b	32 ± 0.7 mm; ^d 258.89 μg/mL ^a	[108]
		<i>E. coli</i> 116 Ag resistant	Citrate partially oxidized	9.2 ± 2.8 nm ^b	>80 nm ^a	[102]
	<i>E. coli</i> 116 Ag sensitive		9.2 ± 2.8 nm ^b	2 nm ^a	[102]	
	<i>E. coli</i> J53 Ag resistant		9.2 ± 2.8 nm ^b	>80 nm ^a	[102]	
	<i>E. coli</i> J53 Ag sensitive		9.2 ± 2.8 nm ^b	2 nm ^a	[102]	
	<i>S. aureus</i>	Gallic acid	20–25 nm ^b	0.7 ± 0.2 μg/mL ^a	[148]	
			Lactose	35 nm ^{a, b}	6.75 μg/mL ^{a, c}	[115]
			Maltose	25 nm ^{a, b}	6.75 μg/mL ^{a, c}	[115]
		PVA	47 nm ^b	Weak activity (8–12 mm) ^d	[149]	
		Gallic acid	7 nm ^{a, b}	7.5 μg/mL ^a	[130]	
			29 nm ^{a, b}	16.67 μg/mL ^a	[130]	
			Citrate	9 ± 2 nm ^b	12 ± 0.4 mm; ^d 14.38 μg/mL ^a	[108]
		Citrate/SDS	30 ± 7 nm ^b	31 ± 1.0 mm; ^d 215.74 μg/mL ^a	[108]	
		SDS	24 ± 6 nm ^b	34 ± 0.5 mm; ^d 258.89 μg/mL ^a	[108]	
<i>S. aureus</i> MRSA	Gallic acid	20–25 nm ^b	0.5 ± 0.2 μg/mL ^a	[148]		
	Lactose	35 nm ^{a, b}	27.0 μg/mL ^{a, c}	[115]		
	Maltose	25 nm ^{a, b}	6.75 μg/mL ^{a, c}	[115]		
Cu	<i>E. coli</i>	Ascorbic acid	5.3 ± 0.1 nm ^{b, c} [8 ppm]	99.9% ^f	[117]	
		<i>S. aureus</i>	Gelatin	56.2 nm, ^a 80 ± 10 nm ^b	4.5 μg/mL, ^a 9.0 μg/mL ^c	[104]
			Ascorbic acid	5.3 ± 0.1 nm ^{b, c} [8 ppm]	86.3% ^f	[117]
		5.3 ± 0.1 nm ^{b, c} [32 ppm]	98.0% ^f	[117]		
CuO	<i>E. coli</i>	HMTA	6 ± 0.5 nm ^b	2.5 μg/mL ^a	[150]	
		PEG	50 nm; ^c 92 nm ^a	1.5 mm; ^d 6.25 μg/mL ^a	[151]	
		<i>S. aureus</i>	PVA	80 ± 20 nm, ^a 50 nm, ^b 70 nm ^d	180 μg/mL, ^a 195 μg/mL ^c	[152]
Selenium	<i>S. aureus</i>	BSA	100 nm, ^a 50 nm ^b	No actual result given (percent/graph)	[153]	
Zinc	<i>E. coli</i>	SDS, Thioglycerol	4 nm ^d	250 μg/mL, ^a 550 μg/mL ^c	[114]	

Notes: Effectiveness: *a*—minimum inhibitory concentration (MIC), *b*—concentration that kills at least 50% (LC50), *c*—minimum bactericidal concentration (MBC), *d*—Zone of inhibition, *e*—half maximal inhibitory concentration (IC50); Size: *a*—dynamic light scattering (DLS), *b*—transmission electron microscope (TEM), *c*—scanning electron microscope (SEM), *d*—Other. Papers not included in this table that focus on antibacterial activity of chemically synthesized particles.^{106, 118, 119, 121, 136, 146–155} All bacteria were treated with NPs in colloidal form.

Table IV. Compilation of results from antibacterial studies of NPs produced via PLAL.

Metal	Bacteria	Form	Chemical additives	Size info (diameter)	Effectiveness	Source		
Ag	Ag-Resistant <i>E. coli</i>	Colloidal in DI H ₂ O	Carbon-coated	In DI H ₂ O: 149.0 ± 89; ^a In MH Media: 501.5 ± 24.2; 27.2 ± 10.3 ^b	No MIC or MBC found viable in 1024.0 ± 0.0 μg/mL ^a	[164]		
				In DI H ₂ O: 167.0 ± 110; ^a In MH Media: 689.4 ± 79.0; ^a 37.0 ± 11.6 ^b	No MIC or MBC found viable in 1024.0 ± 0.0 μg/mL ^a			
	<i>E. coli</i>	Colloidal in acetonitrile	None	None	7 nm ^b	26 nm ^d	[165]	
					Colloidal in DI H ₂ O	5 mM NaCl	100 nm–200 nm ^c	Killed 95% of cells after 3 hours of incubation (cubic structure)
		NPs embedded in agar films	5% PVP	None	9–27 nm ^b	298.7 ± 42.7 μg/mL; ^a 384.0 ± 57.2 μg/mL ^c	384.0 ± 57.2 μg/mL; ^a 469.3 ± 122.2 μg/mL ^c	[164]
						20–25 nm ^b (2 mg/mL) 48–51 nm ^b (16 mg/mL)	2.0 ± 0.09 μg/mL ^a	Ag NP agar plates at concentrations of 0.13, 0.26, and 0.52 mg/mL had 10 ⁶ , 10 ² , and 10 ¹ CFU/mL after incubation of 8 hrs, respectively. The control had 10 ⁹ CFU/mL after 8 hrs of incubation.
		Thin film of Ag- Hydroxyapatite (HA)	None	None	None	Size not determined, surface of morphology of thin film investigated with SEM	Films made with over 0.06 at.% Ag killed >99.9% of cells.	[169]
						Thin film of Ag–SiO ₂	Size not determined, surface of morphology of thin film investigated with SEM	Films made at atomic ratios (Ag:Si) of 19:81, 15:49, and 77:23 produced zones of inhibition of 11, 14, and 15 nm ^d respectively.
		<i>S. aureus</i>	Colloidal in DI H ₂ O	Carbon-coated	None	In DI H ₂ O: 149.0 ± 89; ^a In MH Media: 501.5 ± 24.2; 27.2 ± 10.3 ^b	256.0 ± 0.0 μg/mL; ^a no MBC found viable in 768.0 ± 114.5 μg/mL	[164]
						In DI H ₂ O: 167.0 ± 110; ^a In MH Media: 689.4 ± 79.0; ^a 37.0 ± 11.6 ^b	384.0 ± 57.2 μg/mL; ^a no MBC found viable in 768.0 ± 114.5 μg/mL	
Thin film of Ag–SiO ₂	None		None	None	9–27 nm ^b	5.5 ± 0.27 μg/mL ^a	[167]	
					Size not determined, surface of morphology of thin film investigated with SEM	Films made at atomic ratios (Ag:Si) of 19:81, 15:49, and 77:23 produced zones of inhibition of 16 nm. ^d	[170]	
Cu	<i>E. coli</i>	Colloidal in acetonitrile	None	29.2 nm ^b	35 nm ^d	[165]		
		Colloidal in acetone		3.29 nm ^b	25 nm ^d			
		Colloidal in dichloromethane		2.98 nm ^b	27 nm ^d			
Se	<i>E. coli</i>	Colloidal in DI H ₂ O	None	64 ± 9 nm ^a	Effective against <i>E. coli</i> at concentration of 0.135 ppm	[171]		
				62 ± 12 nm ^a	Effective against <i>E. coli</i> at concentration of 0.135 ppm			
Ni	<i>E. coli</i>		None	50–60 nm ^a	At 21 μM, 29 μM, and 36 μM concentrations the Ni NPs tested were 66%, 86% and 99.92% effective at inhibiting <i>E. coli</i> cell growth.	[172]		
TiO ₂	<i>E. coli</i>			181 nm; ^a 34 ± 1 nm ^c	At a concentration of 100 μg/mL TiO ₂ NPs exposed to light were 85% effective at inhibiting growth of <i>E. coli</i> .	[173]		

Notes: Effectiveness: a—MIC, b—concentration that kills at least 50% (LC50), c—minimum bactericidal concentration (MBC), d—Zone of inhibition, e—half maximal inhibitory concentration (IC50); Size: a—dynamic light scattering (DLS), b—transmission electron microscope (TEM), c—scanning electron microscope (SEM), d—Other Papers not included in this table that focus on antibacterial activity of particles produced by PLAL.^{116, 174–180}

such as superoxide radicals (O_2^-), hydrogen peroxide (H_2O_2), hydroxyl radicals (OH^*), and singlet oxygen (O_2^*).¹¹² Due to the high reactivity of these species, ROS can cause damage to peptidoglycan and cell membranes, DNA, mRNA, ribosomes, and proteins.^{98, 119} ROS can also inhibit transcription, translation, enzymatic activity, and the electron transport chain.^{98, 120, 121} Some metal oxide NPs, such as ZnO, rely on the generation ROS as a main mechanism of toxicity, while Ag NPs are capable of ROS generation as well as Ag ion release.^{97, 113, 114, 122} In general, metal oxide NPs do not show high levels of free ions in solution, so most of the antibacterial effectiveness is thought to be due to ROS production.¹²³ CuO NPs are capable of entering bacterial cells, inactivating enzymes, and generating H_2O_2 , causing cell death.^{116, 124} Some studies have successfully used antioxidants such as *N*-acetylcysteine (NAC) and histidine to prevent ROS from damaging the bacteria.^{114, 125} However, the use of NAC in the Ag NP studies may have inhibited ion interaction and not ROS, due to the binding of free Ag^+ ions to the thiol group of NAC.¹¹⁴ While, ROS generation has been seen in bacterial studies involving only Ag^+ ions,¹²⁶ whether or not the NP or the ion is generating ROS within the cell is still up for debate.

3.3.3. Ion-Mediated

It is believed that NPs can be taken up by bacteria; after the NPs enter the cell they proceed to release metallic ions. As stated in the introduction to this section, metallic salts have long been used as antimicrobial agents. Dissolved metallic salts allow metal ions to complex with numerous proteins, disrupting normal cell function and ultimately causing cell death in some cases (Fig. 4). In the case of Ag NPs, our experience along with others in the literature, shows that the addition of a thiol ligand competes with cellular targets to bind Ag^+ and eliminates any toxic effects.¹²⁷ The binding energy (E_b) of the $Ag^+ - SH$ bond is approximately -1.88 kcal/mol, which is defined as the absolute value of the energy difference $E_b = E_{Ag-SH_2} - (E_{Ag} + E_{SH_2})$.¹²⁸ Consistent with a role for ions in NP toxicity, gene expression analysis indicates that Ag NPs stimulate the upregulation of ion efflux pumps.¹²⁹ The release of ions is also size-dependent, as small particles release a higher percentage of ions into solution.¹⁰⁷ Interestingly, Ivask et al. only measured a 1% release of ions in Ag NP solutions in ultra pure water;¹⁰⁷ however, ion generation did increase slightly when introduced to alternate mediums.¹⁰⁷ These findings may make the fact that NPs bind and become internalized more significant by strongly enhancing the local toxicity of the particles.

Additionally, the NPs may dissolve when in near proximity to or within the cell.¹⁰⁷ In metal oxide NPs, the amount of dissolved ions is concentration-dependent.¹²³ An increase in concentration of metal oxide NPs in lysogeny broth (LB) agar plates resulted in a concomitant decrease in the percentage of free ions.¹²³ Studies show

that the dissolved ion toxicities among the metal oxide NPs CuO, NiO, ZnO and Sb_2O_3 were negligible, which further supports the assertion that metal oxides rely primarily on ROS.¹²³

3.4. Comparison of Wet-Chemistry and PLAL

An attempt was made to determine whether or not there is a benefit to using either chemical synthesis or PLAL when studying the antibacterial effects of NPs. Tables III and IV compile the antimicrobial properties of a variety of NPs. We note that comparison of the various NPs is challenging given the lack of standardized testing methods. As one can see from the tables, there are at least 5 ways to test the antibacterial efficacy of NPs, all producing results that do not have a clear quantitative link.

As an example of the difficulty of making such comparisons, we point to the studies performed by Martinez (29 nm Ag particles)¹³⁰ and Guzman (30 nm Ag particles).¹³¹ While Guzman et al. capped their particles with sodium citrate, Martinez et al. utilized gallic acid as a stabilizing agent. Martinez began with 10^5 colony forming units per milliliter (CFU/mL) and Guzman estimated that $10^5 - 10^6$ CFU/mL were initially present in their study. Given these markedly similar starting conditions, one might expect that a similar minimum inhibitory concentration (MIC) would be found in both studies. However, Martinez found an MIC of approximately $13 \mu\text{g/mL}$, whereas Guzman arrived at a value of approximately $216 \mu\text{g/mL}$. Even allowing for some variation, that can be expected to exist between methodologies in different laboratories, one would not expect such a discrepancy. This may point to the important role of capping agents and ion-release mechanisms like those already discussed for thiols and Ag^+ . It may also point to the need for developing a widely portable protocol for antibacterial studies.

It is typical to observe a higher resistance of Gram-positive bacteria to metallic nanoparticles, compared to that of Gram-negative species. The envelope structure of these two groups of bacteria may play a role in their different tolerances to metallic NPs.^{125, 130} The peptidoglycan cell wall is thicker in Gram-positive strains, which may restrict internalization of the NPs.^{117, 125, 130} Furthermore, some Gram-negative species, such as *S. aureus*, produce alkyl hydroperoxide reductase, catalase, and staphyloxanthin to help defend against ROS.¹¹⁷ At smaller sizes the minimum inhibitory concentration (MIC) is relatively close for both species, but as the size of the particles increases, *S. aureus* exhibit higher resistance than *E. coli*.¹³⁰

Surfactants and stabilizing agents may also be expected to affect the level of NP toxicity. As previously introduced, the charge of a NP can play a role in the adhesion of NPs to cell membranes. The use of cationic or anionic surfactants determines the charge of the nanoparticle.^{132, 133} Polylysine (PL) coated Ag NPs with a positive charge were

compared to 3-mercaptopropionic acid (MPA) coated Ag NPs that were negatively charged.¹³² Surface charges are generally determined by measuring the zeta potential via dynamic light scattering (DLS). Ag NPs 7.2 nm in diameter produced using PL had a zeta potential of 40.2 mV, while NPs with a diameter of 6.7 nm coated with MPA had a zeta potential of -46.1 mV.¹³² Surprisingly, surface charge did not appear to influence AgNP toxicity in this study, implying that electrostatic interactions with the negatively charged bacterial outer-membrane do not play a major role in the antimicrobial effects of silver NPs.¹³² However, this notion of electrostatic interaction is still widely believed to be a mechanism involved in antibacterial efficacy.¹¹² The process of wet-chemical synthesis is highly dependent on the presence of a surfactant or stabilizing agent, while PLAL is capable of producing NPs in the absence of any chemical byproducts, thus producing bare NPs. The benefit of producing bare NPs by PLAL allows for more in depth studies into the effects of NPs on bacterial cells in the absence of surfactants. The ease of production via wet-chemical synthesis will allow for a greater understanding of the effect these surfactants have on NPs and the bacterial cells themselves.

4. CONCLUSION AND OUTLOOK

The two methodologies for producing nanoparticles presented herein provide a broad range of attainable characteristics. This ability to vary properties of both bare and functionalized nanoparticles with high control will ultimately flesh out future studies pertaining to the antibacterial properties of nanoparticles. A direct comparison between NPs produced by wet-chemical methods versus PLAL will be helpful in determining exact antimicrobial mechanisms and trends, which are currently subjects of much discussion in the literature. Nanoparticles have a great potential for furthering studies on the prevention of antibacterial resistance, and for this reason, diligent research in this area is ongoing and will likely only increase in interest in the near future.

Acknowledgments: We would like to thank Kyle Naddeo for the creation of Figures 1 and 2. We would also like to thank the National Science Foundation (NSF) awards CMMI-0922946 to Daniel M. Bubb and CMMI-1300920 to Daniel M. Bubb and Sean M. O'Malley.

References and Notes

1. S. Barcikowski and G. Compagnini, *Phys. Chem. Chem. Phys.* 15, 3022 (2013).
2. H. R. Naika, K. Lingaraju, K. Manjunath, D. Kumar, G. Nagaraju, D. Suresh, and H. Nagabhushana, *J. Taibah Univ. Sci.* 9, 7 (2014).
3. A. Punnoose, K. Dodge, J. W. Rasmussen, J. Chess, D. Wingett, and C. Anders, *ACS Sustain. Chem. Eng.* 2, 1666 (2014).
4. M. N. Nadagouda, N. Iyanna, J. Lalley, C. Han, D. D. Dionysiou, and R. S. Varma, *ACS Sustain. Chem. Eng.* 2, 1717 (2014).
5. R. S. Varma, *Green Chem.* 16, 2027 (2014).
6. P. Anastas and N. Eghbali, *Chem. Soc. Rev.* 39, 301 (2010).
7. V. Amendola and M. Meneghetti, *Phys. Chem. Chem. Phys.* 15, 3027 (2013).
8. H. Zeng, X.-W. Du, S. C. Singh, S. A. Kulinich, S. Yang, J. He, and W. Cai, *Adv. Funct. Mater.* 22, 1333 (2012).
9. S. V. Rao, G. K. Podagatlapalli, and S. Hamad, *J. Nanosci. Nanotechnol.* 14, 1364 (2014).
10. T. Tsuji, D. H. Thang, Y. Okazaki, M. Nakanishi, Y. Tsuboi, and M. Tsuji, *Appl. Surf. Sci.* 254, 5224 (2008).
11. F. Mafune, J. Kohno, Y. Takeda, and T. Kondow, *J. Phys. Chem.* 105, 5114 (2001).
12. M. T. Swihart, *Curr. Opin. Colloid Interface Sci.* 8, 127 (2003).
13. F. E. Kruis, H. Fissan, and A. Peled, *J. Aerosol. Sci.* 29, 511 (1998).
14. H. Hahn, *NanoStructured Mater.* 9, 3 (1997).
15. W. Soliman, T. Nakano, N. Takada, and K. Sasaki, *Jpn. J. Appl. Phys.* 49, 116202-1-116202-1162026 (2010).
16. W. Soliman, N. Takada, and K. Sasaki, *Appl. Phys. Express* 3, 035201-1-035201-035203 (2010).
17. M. E. Povarnitsyn, T. E. Itina, P. R. Levashov, and K. V. Khishchenko, *Phys. Chem. Chem. Phys.* 15, 3108 (2013).
18. S. Ibrahimkuty, P. Wagener, A. Menzel, A. Plech, and S. Barcikowski, *Appl. Phys. Lett.* 101, 103104-1-103104-4 (2012).
19. K. Sasaki, T. Nakano, W. Soliman, and N. Takada, *Appl. Phys. Express* 2, 0465011 (2009).
20. K. Sasaki and N. Takada, *Pure Appl. Chem.* 82, 1317 (2010).
21. N. Haram and N. Ahmad, *Appl. Phys. A* 111, 1131 (2013).
22. M. Amin, J. Tomko, J. J. Naddeo, R. Jimenez, D. M. Bubb, M. Steiner, J. Fitz-Gerald, and S. M. O'Malley, *Appl. Surf. Sci.* 348, 30 (2015).
23. Z. Yan and D. B. Chrisey, *J. Photochem. Photobiol. C Photochem. Rev.* 13, 204 (2012).
24. L. V. Zhigilei, Z. Lin, and D. S. Ivanov, *J. Phys. Chem. C* 113, 11892 (2009).
25. J. D. Blakemore, H. B. Gray, J. R. Winkler, and A. M. Müller, *ACS Catal.* 3, 2497 (2013).
26. K. A. Elsayed, H. Imam, M. A. Ahmed, and R. Ramadan, *Opt. Laser Technol.* 45, 495 (2013).
27. W. T. Nichols, T. Sasaki, and N. Koshizaki, *J. Appl. Phys.* 100, 1 (2006).
28. M. H. Mahdih and B. Fattahi, *Appl. Surf. Sci.* 329, 47 (2015).
29. M. E. Povarnitsyn and T. E. Itina, *Appl. Phys. A Mater. Sci. Process.* 117, 1 (2014).
30. W. T. Nichols, T. Sasaki, and N. Koshizaki, *J. Appl. Phys.* 100, 1 (2006).
31. A. V. Kabashin and M. Meunier, *J. Appl. Phys.* 94, 7941 (2003).
32. T. Tsuji, K. Iryo, N. Watanabe, and M. Tsuji, *Appl. Surf. Sci.* 202, 80 (2002).
33. E. Giorgetti, M. Muniz-Miranda, P. Marsili, D. Scarpellini, and F. Giannanco, *J. Nanoparticle Res.* 14, 1 (2012).
34. A. Schwenke, P. Wagener, S. Nolte, and S. Barcikowski, *Appl. Phys. A Mater. Sci. Process.* 104, 77 (2011).
35. S. Z. Mortazavi, P. Parvin, A. Reyhani, A. N. Golikand, and S. Mirershadi, *J. Phys. Chem. C* 115, 5049 (2011).
36. S. Z. Mortazavi, P. Parvin, A. Reyhani, S. Mirershadi, and R. Sadighi-Bonabi, *J. Phys. D. Appl. Phys.* 46, 1 (2013).
37. J. Kim, D. A. Reddy, R. Ma, and T. K. Kim, *Solid State Sci.* 37, 96 (2014).
38. L. Schlessinger and J. Wright, *Phys. Rev. A* 20, 1934 (1979).
39. S. Z. Shoursheini, P. Parvin, B. Sajad, and M. A. Bassam, *Appl. Spectrosc.* 63, 423 (2009).
40. L. Fornarini, F. Colao, R. Fantoni, V. Lazic, and V. Spizzicchio, *Spectrochim. Acta-Part B* 60, 1186 (2005).
41. B. M. Hunter, J. D. Blakemore, M. Deimund, H. B. Gray, J. R. Winkler, and A. M. Muller, *J. Am. Chem. Soc.* 136, 13118 (2014).
42. K. Maximova, A. Aristov, M. Sentis, and A. V. Kabashin, *Nanotechnology* 26, 1 (2015).

43. D. M. Bubb, S. M. O'Malley, J. Schoeffling, R. Jimenez, B. Zinderman, and S. Yi, *Chem. Phys. Lett.* 565, 65 (2013).
44. P. Chewchinda, T. Tsuge, H. Funakubo, O. Odawara, and H. Wada, *Jpn. J. Appl. Phys.* 52, 1 (2013).
45. L. V. Zhigilei, Z. Lin, and D. S. Ivanov, *J. Phys. Chem. C* 113, 11892 (2009).
46. F. Baset, Ph.D. Thesis, University of Ottawa (2014).
47. S. Sonntag, J. Roth, F. Gaehler, and H. R. Trebin, *Appl. Surf. Sci.* 255, 9742 (2009).
48. Y. Yamashita, T. Yokomine, S. Ebara, and A. Shimizu, *Fusion Eng. Des.* 81, 1695 (2006).
49. C. Momma, B. N. Chichkov, S. Nolte, F. von Alvensleben, A. Tünnermann, H. Welling, and B. Wellegehausen, *Opt. Commun.* 129, 134 (1996).
50. S. Barcikowski, A. Hahn, A. V. Kabashin, and B. N. Chichkov, *Appl. Phys. A* 87, 47 (2007).
51. K. H. Leitz, B. Reddlingshöer, Y. Reg, A. Otto, and M. Schmidt, *Phys. Procedia* 12, 230 (2011).
52. S. M. Eaton, G. Cerullo, and R. Osellame, *Femtosecond Laser Micromachining*, edited by R. Osellame, G. Cerullo, and R. Ramponi, Springer, Berlin (2012), Vol. 123, pp. 287–321.
53. S. Link, C. Burda, M. B. Mohamed, B. Nikoobakht, and M. A. El-Sayed, *J. Phys. Chem. A* 103, 1165 (1999).
54. E. G. Gamaly and A. V. Rode, *Prog. Quantum Electron.* 37, 215 (2013).
55. M. M. Hanon, E. Akman, B. G. Oztoprak, M. Gunes, Z. A. Taha, K. I. Hajim, E. Kacar, O. Gundogdu, and A. Demir, *Opt. Laser Technol.* 44, 913 (2012).
56. F. Dausinger, H. Hugel, and V. Konov, *SPIE Proc.* 5147, 106 (2003).
57. B. Verhoff, S. S. Harilal, J. R. Freeman, P. K. Diwakar, and A. Hassanein, *J. Appl. Phys.* 112, 1 (2012).
58. L. V. Keldysh, *Sov. Phys. J. Exp. Theor. Phys.* 20, 1307 (1965).
59. V. S. Popov, *Physics-Uspexhi* 47, 855 (2004).
60. C. B. Schaffer, A. Brodeur, and E. Mazur, *Meas. Sci. Technol.* 12, 1784 (2001).
61. P. Lambropoulos, *Phys. Rev. Lett.* 55, 2141 (1985).
62. A. Menéndez-Manjón and S. Barcikowski, *Appl. Surf. Sci.* 257, 4285 (2011).
63. C. M. Rouleau, C. Y. Shih, C. Wu, L. V. Zhigilei, A. A. Puretzky, and D. B. Geohegan, *Appl. Phys. Lett.* 104, 1 (2014).
64. L. V. Zhigilei and B. J. Garrison, *Appl. Phys. A* 69, 75 (1999).
65. S. Barcikowski, A. Meñéndez-Manjón, B. Chichkov, M. Brikas, and G. Račiukaitis, *Appl. Phys. Lett.* 91, 20 (2007).
66. F. Mafuné, J.-Y. Kohno, Y. Takeda, and T. Kondow, *J. Am. Chem. Soc.* 125, 1686 (2003).
67. A. Brodeur and S. L. Chin, *J. Opt. Soc. Am. B* 16, 637 (1999).
68. D. Werner, A. Furube, T. Okamoto, and S. Hashimoto, *J. Phys. Chem. C* 115, 8503 (2011).
69. D. Liu, C. Li, F. Zhou, T. Zhang, H. Zhang, X. Li, G. Duan, W. Cai, and Y. Li, *Sci. Rep.* 5, 1 (2015).
70. A. Takami, H. Kurita, and S. Koda, *J. Phys. Chem. B* 103, 1226 (1999).
71. S. Link and M. A. El-Sayed, *J. Phys. Chem. B* 103, 4212 (1999).
72. M. K. Debanath and S. Karmakar, *Mater. Lett.* 111, 116 (2013).
73. B. Swain, H. S. Hong, and H. C. Jung, *Chem. Eng. J.* 264, 654 (2015).
74. J. Turkevich, P. C. Stevenson, and J. Hillier, *Discuss. Faraday Soc.* 11, 55 (1951).
75. D. W. Oxtoby, *Nature* 406, 464 (2000).
76. K. Lu and J. Zhao, *Chem. Eng. J.* 160, 788 (2010).
77. A. S. Ethiraj and D. J. Kang, *Nanoscale Res. Lett.* 7, 1 (2012).
78. J. Zeng, C. Zhu, J. Tao, M. Jin, H. Zhang, Z. Y. Li, Y. Zhu, and Y. Xia, *Angew. Chemie-Int. Ed.* 51, 2354 (2012).
79. B. Wiley, Y. Sun, B. Mayers, and Y. Xia, *Chem.-A Eur. J.* 11, 454 (2005).
80. Y. Xia, Y. Xiong, B. Lim, and S. E. Skrabalak, *Angew. Chemie-Int. Ed.* 48, 60 (2009).
81. N. R. Jana, L. Gearheart, and C. J. Murphy, *J. Phys. Chem. B* 105, 4065 (2001).
82. S. R. K. Perala and S. Kumar, *Langmuir* 29, 9863 (2013).
83. N. R. Jana, L. Gearheart, and C. J. Murphy, *Langmuir* 17, 6782 (2001).
84. W. Niu, L. Zhang, and G. Xu, *Nanoscale* 5, 3172 (2013).
85. Y. Xia, X. Xia, Y. Wang, and S. Xie, *MRS Bull.* 38, 335 (2013).
86. H. Hiramatsu and F. E. Osterloh, *Chem. Mater.* 16, 2509 (2004).
87. Z. S. Pillai and P. V. Kamat, *J. Phys. Chem. B* 108, 945 (2004).
88. G. Frens, *Nat. Phys. Sci.* 241, 20 (1973).
89. M. Biçer and I. Şişman, *Powder Technol.* 198, 279 (2010).
90. H. Hashemipour, M. E. Zadeh, R. Pourakbari, and P. Rahimi, *Int. J. Phys. Sci.* 6, 4331 (2011).
91. Y. Qin, X. Ji, J. Jing, H. Liu, H. Wu, and W. Yang, *Colloids Surfaces A Physicochem. Eng. Asp.* 372, 172 (2010).
92. A. Zielińska, E. Skwarek, A. Zaleska, M. Gazda, and J. Hupka, *Procedia Chem.* 1, 1560 (2009).
93. H. Wang, X. Qiao, J. Chen, and S. Ding, *Colloids Surfaces A Physicochem. Eng. Asp.* 256, 111 (2005).
94. M. L. Kahn, M. Monge, V. Collière, F. Senocq, A. Maisonnat, and B. Chaudret, *Adv. Funct. Mater.* 15, 458 (2005).
95. A. Ivask, A. Elbadawy, C. Kaweeteerawat, D. Boren, H. Fischer, Z. Ji, C. H. Chang, R. Liu, T. Tolaymat, D. Telesca, J. I. Zink, Y. Cohen, P. A. Holden, and H. A. Godwin, *ACS Nano* 8, 374 (2014).
96. J. W. Alexander, *Surg. Infect. (Larchmt)*. 10, 289 (2009).
97. L. Zhang, Y. Jiang, Y. Ding, N. Daskalakis, L. Jeuken, M. Povey, A. J. O'Neill, and D. W. York, *J. Nanoparticle Res.* 12, 1625 (2010).
98. R. Y. Pelgrift and A. J. Friedman, *Adv. Drug Deliv. Rev.* 65, 1803 (2013).
99. C. A. Arias and B. E. Murray, *N. Engl. J. Med.* 372, 1168 (2015).
100. J.-M. Ahn, H.-J. Eom, X. Yang, J. N. Meyer, and J. Choi, *Chemosphere* 108, 343 (2014).
101. H. J. Eom, J. M. Ahn, Y. Kim, and J. Choi, *Toxicol. Appl. Pharmacol.* 270, 106 (2013).
102. C. N. Lok, C. M. Ho, R. Chen, Q. Y. He, W. Y. Yu, H. Sun, P. K. H. Tam, J. F. Chiu, and C. M. Che, *J. Biol. Inorg. Chem.* 12, 527 (2007).
103. O. Choi and Z. Hu, *Environ. Sci. Technol.* 42, 4583 (2008).
104. A. K. Chatterjee, R. K. Sarkar, A. P. Chattopadhyay, P. Aich, R. Chakraborty, and T. Basu, *Nanotechnology* 23, 1 (2012).
105. J. R. Morones, J. L. Elechiguerra, A. Camacho, K. Holt, J. B. Kouri, J. T. Ramírez, and M. J. Yacaman, *Nanotechnology* 16, 2346 (2005).
106. L. Rizzello and P. P. Pompa, *Chem. Soc. Rev.* 43, 1501 (2014).
107. A. Ivask, I. Kurvet, K. Kasemets, I. Blinova, V. Aruoja, S. Suppi, H. Vija, A. Kärinen, T. Titma, M. Heinlaan, M. Visnapuu, D. Koller, V. Kisand, and A. Kahru, *PLoS One* 9, 1 (2014).
108. M. Guzman, J. Dille, and S. Godet, *Nanomedicine Nanotechnology, Biol. Med.* 8, 37 (2012).
109. A. Azam, A. S. Ahmed, M. Oves, M. S. Khan, and A. Memic, *Int. J. Nanomedicine* 7, 3527 (2012).
110. T. H. Kim, M. Kim, H. S. Park, U. S. Shin, M. S. Gong, and H. W. Kim, *J. Biomed. Mater. Res.-Part A* 100 A, 1033 (2012).
111. K. R. Raghupathi, R. T. Koodali, and A. C. Manna, *Langmuir* 27, 4020 (2011).
112. C. You, C. Han, X. Wang, Y. Zheng, Q. Li, X. Hu, and H. Sun, *Mol. Biol. Rep.* 39, 9193 (2012).
113. S. Prabhu and E. K. Poulou, *Int. Nano Lett.* 2, 1 (2012).
114. R. K. Dutta, B. P. Nenavathu, M. K. Gangishetty, and A. V. R. Reddy, *Colloids Surfaces B Biointerfaces* 94, 143 (2012).
115. A. Panáček, L. Kvítek, R. Prucek, and M. Kolar, R. Vecerova, N. Pizúrova, V. K. Sharma, and T. Nevecna, and R. Zbořil, *J. Phys. Chem. B* 110, 16248 (2006).

116. A. Nath, A. Das, L. Rangan, and A. Khare, *Sci. Adv. Mater.* 4, 1 (2012).
117. U. Bogdanović, V. Lazić, V. Vodnik, M. Budimir, Z. Marković, and S. Dimitrijević, *Mater. Lett.* 128, 75 (2014).
118. N. Hoshino, T. Kimura, A. Yamaji, and T. Ando, *Free Radic. Biol. Med.* 27, 1245 (1999).
119. H. Sies, *Exp. Physiol.* 82, 291 (1997).
120. M. Raffi, F. Hussain, T. M. Bhatti, J. I. Akhter, A. Hameed, and M. M. Hasan, *J. Mater. Sci. Technol.* 24, 192 (2008).
121. H. Sies, *Exp. Physiol.* 82, 291 (1996).
122. O. Choi, K. K. Deng, N. J. Kim, L. Ross, R. Y. Surampalli, and Z. Hu, *Water Res.* 42, 3066 (2008).
123. Y. W. Baek and Y. J. An, *Sci. Total Environ.* 409, 1603 (2011).
124. A. P. Ingle, N. Duran, and M. Rai, *Appl. Microbiol. Biotechnol.* 98, 1001 (2014).
125. J. S. Kim, E. Kuk, K. N. Yu, J.-H. Kim, S. J. Park, H. J. Lee, S. H. Kim, Y. K. Park, Y. H. Park, C.-Y. Hwang, Y.-K. Kim, Y.-S. Lee, D. H. Jeong, and M.-H. Cho, *Nanomedicine* 3, 95 (2007).
126. H.-J. Park, J. Y. Kim, J. Kim, J.-H. Lee, J.-S. Hahn, M. B. Gu, and J. Yoon, *Water Res.* 43, 1027 (2009).
127. J. Y. Kim, C. Lee, M. Cho, and J. Yoon, *Water Res.* 42, 356 (2008).
128. A. H. Pakiari and Z. Jamshidi, *J. Phys. Chem. A* 114, 9212 (2010).
129. A. Nagy, A. Harrison, S. Sabbani, R. S. Munson, P. K. Dutta, and W. J. Waldman, *Int. J. Nanomedicine* 6, 1833 (2011).
130. G. A. Martínez-Castanon, N. Niño-Martínez, F. Martínez-Gutiérrez, J. R. Martínez-Mendoza, and F. Ruiz, *J. Nanoparticle Res.* 10, 1343 (2008).
131. M. G. Guzmán, J. Dille, and S. Godet, *Int. J. Chem.* 2, 104 (2009).
132. A. Dror-Ehreh, H. Mamane, T. Belenkova, G. Markovich, and A. Adin, *J. Colloid Interface Sci.* 339, 521 (2009).
133. A. M. El Badawy, K. G. Scheckel, M. Suidan, and T. Tolaymat, *Sci. Total Environ.* 429, 325 (2012).
134. V. K. LaMer and R. H. Dinegar, *J. Am. Chem. Soc.* 72, 4847 (1950).
135. J. G. Eberhart and S. Horner, *J. Chem. Educ.* 87, 608 (2010).
136. K. Nouneh, M. Oyama, R. Diaz, M. Abd-Lefdil, I. V. Kityk, and M. Bousmina, *J. Alloys Compd.* 509, 2631 (2011).
137. J. Chang and E. R. Waclawik, *Cryst. Eng. Comm.* 15, 5612 (2013).
138. S. Chandrasekaran, *Sol. Energy Mater. Sol. Cells* 109, 220 (2013).
139. I. Lisiecki, F. Billoudet, and M. P. Pileni, *J. Phys. Chem.* 100, 4160 (1996).
140. X. Xia, L. Figueroa-Cosme, J. Tao, H. C. Peng, G. Niu, Y. Zhu, and Y. Xia, *J. Am. Chem. Soc.* 136, 10878 (2014).
141. S. Guo and E. Wang, *J. Colloid Interface Sci.* 315, 795 (2007).
142. C. Cheng, S. Gong, Q. Fu, L. Shen, Z. Liu, Y. Qiao, and C. Fu, *Polym. Bull.* 66, 735 (2011).
143. T. Dadosh, *Mater. Lett.* 63, 2236 (2009).
144. H. Kumarakuru, M. J. Coombes, J. H. Neethling, and J. E. Westraadt, *J. Alloys Compd.* 589, 67 (2014).
145. K. Xu, J. X. Wang, X. L. Kang, and J. F. Chen, *Mater. Lett.* 63, 31 (2009).
146. I. Sondi, D. V. Goia, and E. Matijević, *J. Colloid Interface Sci.* 260, 75 (2003).
147. J. S. Bozich, S. E. Lohse, M. D. Torelli, C. J. Murphy, R. J. Hamers, and R. D. Klapper, *Environ. Sci. Nano* 1, 260 (2014).
148. F. Martínez-Gutiérrez, P. L. Olive, A. Banuelos, E. Orrantia, N. Nino, E. M. Sanchez, F. Ruiz, H. Bach, and Y. Av-Gay, *Nanomedicine Nanotechnology, Biol. Med.* 6, 681 (2010).
149. I. O. Ali, *Colloids Surfaces A Physicochem. Eng. Asp.* 436, 922 (2013).
150. M. S. Hassan, T. Amna, O.-B. Yang, M. H. El-Newehy, S. S. Al-Deyab, and M.-S. Khil, *Colloids Surfaces B Biointerfaces* 97, 201 (2012).
151. A. Ananth, S. Dharaneedharan, M. S. Heo, and Y. S. Mok, *Chem. Eng. J.* 262, 179 (2015).
152. R. Chakraborty, R. K. Sarkar, A. K. Chatterjee, U. Manju, A. P. Chattopadhyay, and T. Basu, *Biochim. Biophys. Acta* 1850, 845 (2015).
153. P. A. Tran and T. J. Webster, *Int. J. Nanomedicine* 6, 1553 (2011).
154. S. Kheybari, N. Samadi, S. V. Hosseini, A. Fazeli, and M. R. Fazeli, *Daru* 18, 168 (2010).
155. W. R. Li, X. B. Xie, Q. S. Shi, H. Y. Zeng, Y. S. Ou-Yang, and Y. B. Chen, *Appl. Microbiol. Biotechnol.* 85, 1115 (2010).
156. S. Pal, Y. K. Tak, and J. M. Song, *Appl. Environ. Microbiol.* 73, 1712 (2007).
157. J. Ramyadevi, K. Jeyasubramanian, A. Marikani, G. Rajakumar, and A. A. Rahuman, *Mater. Lett.* 71, 114 (2012).
158. J. P. Ruparelia, A. K. Chatterjee, S. P. Duttagupta, and S. Mukherji, *Acta Biomater.* 4, 707 (2008).
159. S. Sarkar, A. D. Jana, S. K. Samanta, and G. Mostafa, *Polyhedron* 26, 4419 (2007).
160. S. Shrivastava, T. Bera, A. Roy, G. Singh, P. Ramachandrarao, and D. Dash, *Nanotechnology* 18, 225103 (2007).
161. S. Sivakumar, A. Venkatesan, P. Soundhirarajan, and C. P. Khatiwada, *Spectrochim. Acta Part A Mol. Biomol. Spectrosc.* 136, 1751 (2015).
162. I. Sondi and B. Salopek-Sondi, *J. Colloid Interface Sci.* 275, 177 (2004).
163. D. Wu, Z. Chen, K. Cai, D. Zhuo, J. Chen, and B. Jiang, *Curr. Appl. Phys.* 14, 1470 (2014).
164. M. E. Samberg, P. E. Orndorff, and N. A. Monteiro-Riviere, *Nanotoxicology* 5, 244 (2011).
165. H. Syed, G. K. Podagatlapalli, A. Hussian, N. Ahmed, S. Sreedhar, S. P. Tewari, and S. V. Rao, *Int. Conf. Fiber Opt. Photonics* 1 (2012).
166. C. Dong, Z. Yan, J. Kokx, D. B. Chrisey, and C. Z. Dinu, *Appl. Surf. Sci.* 258, 9218 (2012).
167. J. K. Pandey, R. K. Swarnkar, K. K. Soumya, P. Dwivedi, M. K. Singh, S. Sundaram, and R. Gopal, *Appl. Biochem. Biotechnol.* 174, 1021 (2014).
168. J. W. Rhim, L. F. Wang, Y. Lee, and S. I. Hong, *Carbohydr. Polym.* 103, 456 (2014).
169. M. Jilinek, T. Kocourek, J. Remsa, M. Weiserová, K. Jurek, J. Mikšovský, J. Strnad, A. Galandáková, and J. Ulrichová, *Mater. Sci. Eng. C* 33, 1242 (2013).
170. L. Lei, X. Liu, Y. Yin, Y. Sun, M. Yu, and J. Shang, *Mater. Lett.* 130, 79 (2014).
171. G. Guisbiers, Q. Wang, E. Khachatryan, M. J. Arellano-Jimenez, T. J. Webster, P. Larese-Casanova, and K. L. Nash, *Laser Phys. Lett.* 12, 016003 (2015).
172. S. Shamaila, H. Wali, R. Sharif, J. Nazir, N. Zafar, and M. S. Rafique, *Appl. Phys. Lett.* 103, 153701 (2013).
173. M. Zimbone, M. A. Buccheri, G. Cacciato, R. Sanz, G. Rappazzo, S. Boninelli, R. Reitano, L. Romano, V. Privitera, and M. G. Grimaldi, *Appl. Catal. B Environ.* 165, 487 (2015).
174. A. Ancona, M. C. Sportelli, A. Trapani, R. A. Picca, C. Palazzo, E. Bonerba, F. P. Mezzapesa, G. Tantillo, G. Trapani, and N. Cioffi, *Mater. Lett.* 136, 397 (2013).
175. E. Fadeeva, V. K. Truong, M. Stiesch, B. N. Chichkov, R. J. Crawford, J. Wang, and E. P. Ivanova, *Langmuir* 27, 3012 (2011).
176. S. Grade, J. Eberhard, J. Jakobi, A. Winkel, M. Stiesch, and S. Barcikowski, *Gold Bull.* 47, 83 (2014).
177. Y. F. Joya, Z. Liu, K. S. Joya, and T. Wang, *Nanotechnology* 23, 495708 (2012).
178. K. Krishnamoorthy, N. Umasuthan, R. Mohan, J. Lee, and S. J. Kim, *Sci. Adv. Mater.* 4, 1 (2012).
179. D. Longano, N. Ditaranto, N. Cioffi, F. Di Niso, T. Sibillano, A. Ancona, A. Conte, M. A. Del Nobile, L. Sabbatini, and L. Torsi, *Anal. Bioanal. Chem.* 403, 1179 (2012).
180. S. H. Stelzig, C. Menneking, M. S. Hoffmann, K. Eisele, S. Barcikowski, M. Klapper, and K. Müllen, *Eur. Polym. J.* 47, 662 (2011).

Received: 2 April 2015. Accepted: 7 June 2015.